White Rose Research Online

eprints@whiterose.ac.uk
https://eprints.whiterose.ac.uk
Universities of Leeds, Sheffield and York

Deposited via The University of Leeds.

White Rose Research Online URL for this paper:
https://eprints.whiterose.ac.uk/id/eprint/185478/

Version: Accepted Version

Article:
Rocha de Faria, J, Lesnic, D, da Silva Lima, R et al. (2022) The method of fundamental solutions for pointwise source reconstruction. Computers and Mathematics with Applications, 114. pp. 171-179. ISSN: 0898-1221

https://doi.org/10.1016/j.camwa.2022.03.041

© 2022 Elsevier Ltd. This manuscript version is made available under the CC-BY-NC-ND 4.0 license http://creativecommons.org/licenses/by-nc-nd/4.0/.

Reuse
This article is distributed under the terms of the Creative Commons Attribution-NonCommercial-NoDerivs (CC BY-NC-ND) licence. This licence only allows you to download this work and share it with others as long as you credit the authors, but you can't change the article in any way or use it commercially. More information and the full terms of the licence here: https://creativecommons.org/licenses/

Takedown
If you consider content in White Rose Research Online to be in breach of UK law, please notify us by emailing eprints@whiterose.ac.uk including the URL of the record and the reason for the withdrawal request.

UNIVERSITY OF LEEDS
University of Sheffield
UNIVERSITY of York

The method of fundamental solutions for pointwise source reconstruction

Jairo Rocha de Faria[a], Daniel Lesnic[b], Rômulo da Silva Lima[a], and Thiago José Machado[a]

[a] *Universidade Federal da Paraíba, João Pessoa, Paraíba, Brasil*
[b] *Department of Applied Mathematics, University of Leeds, Leeds, LS2 9JT, UK*

Abstract

This work deals with the reconstruction of point sources in the modified Helmholtz equation in two and three dimensions. This problem has critical applications in engineering and medicine, such as the identification of dipoles and monopoles in electroencephalography and magnetoencephalography and locating sources of environmental pollution. From the numerical point of view, we apply the method of fundamental solutions to solve the direct problems arising from the sensitivity analysis. In addition to the recognized advantages of this meshless spectral method over the traditional mesh-based numerical methods, this approach represents the pointwise sources adequately. Our numerical examples show that the algorithm is capable of accurate reconstruction even when noisy data are inverted.

Keywords: Inverse Problems, Pointwise Source, Sensitivity Analysis, Method of Fundamental Solutions, Modified Helmholtz Equation

1. Introduction

The aim of this work is to propose a stable, reliable and efficient reconstruction algorithm for the solution of an inverse source problem for the modified Helmholtz equation governing steady-state diffusion-reaction phenomena. This inverse problem presents relevant applications, among which we can point out: identification of pollution sources in a river based on chemical and biological oxygen demand [15]; reconstruction of source term of accidental release of atmospheric pollutant [32]; susceptibility map reconstruction of brain images [12]; computed tomography and ultrasound [10];

reconstruction tomography for optical molecular imaging, aiding in cancer diagnosis and nondestructive tests on components [25].

In related work, Machado et al. [28] conducted a study of the pointwise source reconstruction from a single set of boundary Cauchy data in the two-dimensional Laplace's/Poisson's equation using the finite elements method (FEM) [33]. In the present work, we extend the analysis of [29] to the modified Helmholtz equation (as a lower-order perturbation of the Laplacian). Furthermore, instead of discretization domain FEM, taking into account the suitable representation of pointwise sources, we apply the method of fundamental solutions (MFS) in order to solve the associated direct problems. The advantages of this meshless numerical technique over methods of discretization are the ease and simplicity of implementation, rapid convergence and high accuracy [20, 21]. We also minimize a least-squares boundary integral instead of the Kohn-Vogelius domain integral as in [28, 6].

We perform numerical tests to analyze the proposed methodology in two and three dimensions inverting noisy data for reconstruction of up to three-point sources.

The paper is structured as follows. In Section 2, we present the mathematical formulation of the inverse problem and the associated optimization problem. In Section 3, we perform a sensitivity analysis of the shape functional that is minimized. Section 4 discusses the adaptation of the MFS made in this work to represent the pointwise sources considering singularities within the solution domain. In Section 5, the results of numerical experiments are presented and discussed. Finally, in Section 6 we provide some conclusions and discuss some proposals for future work.

2. Mathematical Formulation

2.1. The inverse problem

Let $\Omega \subset \mathbb{R}^d$, $d = 2, 3$, be an open and bounded domain with Lipschitz boundary. Consider the following overdetermined boundary value problem

$$\left\{ \begin{array}{rcll} (\lambda I - \Delta) z & = & b^* & \text{in} \quad \Omega, \\ z & = & u^* \\ -\partial_n z & = & q^* \end{array} \right\} \text{on} \quad \partial\Omega, \tag{1}$$

where λ is a given positive constant and $\underline{n}$ is the unit normal to the boundary $\partial\Omega$. The elliptic linear partial differential equation in (1) is called the modified Helmholtz equation and it governs steady-state reaction-diffusion

processes. In this work, the constant λ is considered strictly positive and it is called the intensity of reaction. We highlight that when $\lambda = 0$ we have the Laplace equation and when $\lambda < 0$ we obtain the Helmholtz equation. Convective/advective terms of the form $\underline{v}_f \cdot \nabla z$, where $\underline{v}_f$ is the fluid velocity of the flow propagating through the medium Ω, can also be added to the governing equation [17].

The underlying inverse problem consists of finding the unknown source b^* in Ω from the Cauchy data u^* and q^* on $\partial\Omega$. In general, this problem has no unique solution. However, if we consider the set of admissible pointwise sources:

$$C_\delta(\Omega) = \left\{ \begin{array}{l} b \in L^1(\Omega), \text{ for which there exists } n \in \mathbb{N}\backslash\{0\}, \alpha_1, \ldots, \alpha_n \in \mathbb{R} \\ \text{and } \underline{y}_1, \ldots, \underline{y}_n \in \Omega \text{ such that } b(\underline{x}) = \displaystyle\sum_{i=1}^{n} \alpha_i \delta(\underline{x} - \underline{y}_i) \end{array} \right\}, \tag{2}$$

where δ is the Dirac-delta generalized function, then the inverse problem (1) has at most one solution $b^* \in C_\delta(\Omega)$, see [15, 16, 17]. The pointwise source b^*, solution of the inverse problem (1), belongs to $C_\delta(\Omega)$ and, therefore, has the representation

$$b^*(\underline{x}) = \sum_{i=1}^{m^*} \alpha_i^* \delta(\underline{x} - \underline{y}_i^*), \tag{3}$$

where $m^* \in \mathbb{N}\backslash\{0\}$, $\underline{\alpha}^* = (\alpha_1^*, \ldots, \alpha_{m^*}^*) \in \mathbb{R}^{m^*}$ and $\underline{y}^* = (\underline{y}_1^*, \ldots, \underline{y}_{m^*}^*) \in \Omega^{m^*}$ denote, respectively, the number, intensities and locations of the pointwise source b^*. The objective is to reconstruct parameters m^*, $\underline{\alpha}^*$ and $\underline{y}^*$. Similar inverse pointwise source identification problems can be considered for the advection-diffusion-reaction equation [17], the Stokes equations of slow viscous flow [2], the heat equation [26, 14] and the wave equation [13].

Let $\mathcal{M}(\Omega)$ be the set of real and regular Borel measures equipped with the following norm [9]:

$$\|\mu\|_{\mathcal{M}(\Omega)} = \sup \left\{ \int_\Omega \varphi \, d\mu; \varphi \in C^0(\Omega) \text{ and } \|\varphi\|_\infty = 1 \right\}, \tag{4}$$

where $\|\cdot\|_\infty$ denotes the supremum norm defined on the set $C^0(\Omega)$ of continuous functions with compact support, namely, $\|\varphi\|_\infty = \sup_{\underline{x} \in \Omega} |\varphi(\underline{x})|$. According

to Riesz representation theorem, $\mathcal{M}(\Omega)$ is the dual space of $C^0(\Omega)$. It is possible to demonstrate that $C_\delta(\Omega) \subset \mathcal{M}(\Omega)$.

2.2. The optimization problem

Next, we consider an optimization problem equivalent to the inverse problem (1). Let us consider Cauchy data pair (u^*, q^*). First, we use q^* to define a Neumann condition for a direct auxiliary problem whose source term is an element of the set of admissible pointwise sources $C_\delta(\Omega)$ defined in (2). In other words, we have the following boundary value problem:

$$\left\{ \begin{array}{rcl} (\lambda I - \Delta)u & = & b_0 \quad \text{in} \quad \Omega, \\ -\partial_n u & = & q^* \quad \text{on} \quad \partial\Omega. \end{array} \right. \tag{5}$$

The source term b_0 is taken arbitrarily in $C_\delta(\Omega)$. In addition, the Dirichlet data u^* is used to define the least-squares functional

$$\mathcal{J}(u) = \frac{1}{2} \int_{\partial\Omega} (u - u^*)^2 \, ds, \tag{6}$$

Note that the functional (6) implicitly depends on the source term b_0 through the problem (5). In this way, the optimization problem that we want to solve consists of minimizing this functional within the admissible set $C_\delta(\Omega)$ of pointwise sources. In other words, we are looking for a source term $b^{opt} \in C_\delta(\Omega)$ such that

$$b^{opt} = \underset{b_0 \in C_\delta(\Omega)}{\arg\min} \, \mathcal{J}(u). \tag{7}$$

In order to show the equivalence between the inverse problem (1) and the optimization problem (7) it is necessary to ensure that the functional (6) has an unique minimum in the set $C_\delta(\Omega)$ and, furthermore, to obtain that $b^{opt} = b^*$. The result enunciated and demonstrated in Proposition 1 guarantees that the functional (6) reaches a minimum value when evaluated at the solution of the inverse problem.

Proposition 1. *Let u be solution of the problem* (5) *and let b^* be the unknown pointwise source of the inverse problem* (1)*. If $b_0 = b^*$, then $\mathcal{J}(u) = 0$.*

Proof. Define $\Psi = u - z$, where z is the solution to problem (1). Then, Ψ is the solution of the following boundary value problem:

$$\left\{ \begin{array}{rcl} (\lambda I - \Delta)\Psi & = & 0 \quad \text{in} \quad \Omega, \\ -\partial_n \Psi & = & 0 \quad \text{on} \quad \partial\Omega, \end{array} \right. \tag{8}$$

After multiplying the differential equation by Ψ and using integration by parts, we have

$$\int_\Omega \left(\lambda\Psi^2 + |\nabla\Psi|^2\right) dx = 0. \tag{9}$$

We have that $\Psi \equiv 0$ on Ω provided that $\lambda > 0$. Therefore, $u = z$, which concludes the proof. □

Although the above result is trivial and has a standard demonstration, we keep it in the text for the sake of completeness. In fact, the result presented in Proposition 2 is much more relevant, as it provides the regularity of the solution to the direct problem (5) and an estimate of this solution as a function of the source term.

Proposition 2. *Let $b_0 \in \mathcal{M}(\Omega)$ and $u \in L^2(\Omega)$ be such that*

$$\int_\Omega u(-\Delta\varphi + \lambda\varphi)\, dx = \int_\Omega b_0\varphi\, dx, \quad \forall\varphi \in H^2(\Omega) \cap H_0^1(\Omega). \tag{10}$$

Then, $u \in W_0^{1,p}(\Omega)$ for all $p \in \left[1, \dfrac{d}{d-1}\right)$ and there exists $D_p > 0$ such that

$$\|u\|_{W_0^{1,p}(\Omega)} \leq D_p \|b_0\|_{\mathcal{M}(\Omega)}. \tag{11}$$

Proof. The proof can be found in [8]. □

3. Sensitivity Analysis

3.1. Perturbed problems

In this section, we perform an arbitrary perturbation on the source b_0 in order to evaluate the sensitivity of the functional (6) with respect to the set of admissible sources $C_\delta(\Omega)$. Namely, we introduce m arbitrary pointwise sources with locations $\underline{y}_i$ and intensities α_i, which provides the following perturbed source:

$$b_\delta(\underline{x}) = b_0(\underline{x}) + \sum_{i=1}^{m} \alpha_i \delta(\underline{x} - \underline{y}_i), \tag{12}$$

Note that $b_\delta \in C_\delta(\Omega)$. The perturbation on the source of problem (5) provides the following perturbed boundary value problem:

$$\left\{ \begin{array}{rcll} (\lambda I - \Delta)u_\delta & = & b_\delta & \text{in} \quad \Omega, \\ -\partial_n u_\delta & = & q^* & \text{on} \quad \partial\Omega. \end{array} \right. \tag{13}$$

Therefore, the perturbed counterpart of the functional (6) is given by

$$\mathcal{J}(u_\delta) \;=\; \frac{1}{2}\int_{\partial\Omega}(u_\delta - u^*)^2 ds. \tag{14}$$

The objective is to evaluate the variation of the functional (6) with respect to the parameters m, $\underline{y} = (\underline{y}_1, \ldots, \underline{y}_m)$ and $\underline{\alpha} = (\alpha_1, \ldots, \alpha_m)$, which define the perturbation on the functional. For this purpose, let us initially consider the following relation between solutions to problems (5) and (13):

$$u_\delta(\underline{x}) = u(\underline{x}) + v(\underline{x}). \tag{15}$$

Then, we have that

$$(\lambda I - \Delta)v(\underline{x}) = \sum_{i=1}^{m} \alpha_i \delta(\underline{x} - \underline{y}_i). \tag{16}$$

Equation (16) implies that, besides spatial variable $\underline{x}$, the function v also depends on the variables m, $\underline{y}$ and $\underline{\alpha}$. Let us consider the following decomposition of v:

$$v(\underline{x}) = \sum_{i=1}^{m} \alpha_i v_i(\underline{x}). \tag{17}$$

Consequently, we have that the function v_i depends only on the spatial variable $\underline{x}$ and on the locations $\underline{y}_i$, for $i = 1, \cdots, m$. It follows that each v_i is the solution to the following boundary value problem:

$$\left\{ \begin{array}{rcll} (\lambda I - \Delta)v_i & = & \delta(\cdot - \underline{y}_i) & \text{in} \quad \Omega, \\ -\partial_n v_i & = & 0 & \text{on} \quad \partial\Omega. \end{array} \right. \tag{18}$$

Proposition 3. *The set $\{v_1, \ldots, v_m\}$ consists of linearly independent functions.*

Proof. Consider $c_1, \ldots, c_m \in \mathbb{R}$ such that

$$c_1 v_1(\underline{x}) + \ldots + c_m v_m(\underline{x}) = 0, \quad \forall \underline{x} \in \Omega. \tag{19}$$

By applying the differential operator $(\lambda I - \Delta)$ on both sides of the above equation, it follows that

$$\begin{array}{rcl} 0 & = & (\lambda I - \Delta)(c_1 v_1(\underline{x}) + \ldots + c_m v_m(\underline{x})) \\ & = & c_1 \delta(\underline{x} - \underline{y}_1) + \ldots + c_m \delta(\underline{x} - \underline{y}_m), \end{array}$$

for all $\underline{x} \in \Omega$. In particular, by taking $\underline{x} = \underline{y}_i$ it is possible conclude that $c_i = 0$ for each $i = 1, \ldots, m$, which concludes the proof. □

3.2. Variation of the functional

We can now calculate the variation of functional (6). Considering the expression (15) and using it in (14), we obtain:

$$\mathcal{J}(u_\delta) = \mathcal{J}(u) + \int_{\partial\Omega} \left(\sum_{i=1}^{m} \alpha_i v_i \right) (u - u^*)\, ds + \frac{1}{2} \int_{\partial\Omega} \left(\sum_{i=1}^{m} \alpha_i v_i \right)^2 ds. \quad (20)$$

Note that the expression on the right hand side of (20) depends explicitly on parameters m and α_i, for $i = 1, \ldots, m$. On the other hand, it depends implicitly on $\underline{y}_i$ through functions v_i, for $i = 1, \ldots, m$. Then, we can rewrite it as follows:

$$\mathcal{J}(u_\delta) - \mathcal{J}(u) = J(m, \underline{\alpha}, \underline{y}). \quad (21)$$

In order to simplify the notation, let us define the vector $\underline{\mathrm{d}} \in \mathbb{R}^m$ and the matrix $H \in \mathbb{R}^{m \times m}$ whose entries are defined by:

$$\mathrm{d}_i = \int_{\partial\Omega} v_i (u - u^*)\, ds, \quad (22)$$

and

$$H_{ij} = \int_{\partial\Omega} v_i\, v_j\, ds. \quad (23)$$

Then, we can rewrite (21) in the following matrix representation [29]:

$$J(m, \underline{\alpha}, \underline{y}) = \underline{\mathrm{d}} \cdot \underline{\alpha}^T + \frac{1}{2} \underline{\alpha} \cdot H \underline{\alpha}^T. \quad (24)$$

Proposition 4. *The matrix H is symmetric and positive definite.*

Proof. The symmetry of H follows straight from definition (23). Let $\underline{\xi} = (\xi_1, \ldots, \xi_m) \in \mathbb{R}^m$ be an arbitrary vector. Note that:

$$\underline{\xi} \cdot H \underline{\xi}^T = \int_{\partial\Omega} \left(\sum_{i=1}^{m} \xi_i v_i \right)^2 ds \geq 0. \quad (25)$$

Suppose that $\underline{\xi}^0 \cdot H (\underline{\xi}^0)^T = 0$ for some $\underline{\xi}^0 \in \mathbb{R}^m$. Clearly, we can conclude that:

$$\sum_{i=1}^{m} \xi_i^0 v_i = 0. \quad (26)$$

It follows from Proposition 3 that $\underline{\xi}^0 \equiv 0$. □

Since H is a symmetric and positive definite matrix, then $J(m, \underline{\alpha}, \underline{y})$ is strictly convex with respect to the parameter $\underline{\alpha}$. In other words, for fixed values of m and $\underline{y}$, there is a global minimum $\widehat{\underline{\alpha}}$, which is obtained by solving the following system:

$$\left\langle D_\alpha J(m, \widehat{\underline{\alpha}}, \underline{y}), \underline{\beta} \right\rangle = 0, \quad \forall \underline{\beta} \in \mathbb{R}^m, \tag{27}$$

where $D_\alpha J$ is the Jacobian of J with respect to $\underline{\alpha}$. Solving (27) and considering the symmetry of H, we have

$$H \widehat{\underline{\alpha}}^T = -\underline{\mathrm{d}}^T. \tag{28}$$

Since H and $\underline{\mathrm{d}}$ depend on the functions v_i, which in turn depend on the locations vector $\underline{y}$, then it is possible to conclude that $\widehat{\underline{\alpha}} = \widehat{\underline{\alpha}}(\underline{y}) = -H^{-1}(\underline{\mathrm{d}}^T)$. Introducing this into (24), the optimal locations $\underline{y}^{opt}$ can be obtained by a combinatorial search over the domain Ω. These locations are solutions to the following minimization problem:

$$\underline{y}^{opt} = \underset{\underline{y} \in X}{\operatorname{argmin}} \left\{ J(m, \widehat{\underline{\alpha}}(\underline{y}), \underline{y}) = \frac{1}{2} \widehat{\underline{\alpha}}(\underline{y}) \cdot \underline{\mathrm{d}}^T \right\}, \tag{29}$$

where $X \subset \Omega$ is a set of admissible source locations of size $\#X \geq m$. In practice, X is a set grid points in the problem domain Ω. Finally, the vector of optimal intensities is given by $\underline{\alpha}^{opt} = \widehat{\underline{\alpha}}(\underline{y}^{opt})$. Since the functional J is strictly convex with respect to the variable $\underline{\alpha}$, then the optimization process defined by Eqs. (28) and (29) provide a global minimum, regardless of the initial guess.

It is important to emphasize that, for a fixed m, it is possible to obtain a pair of optimal solutions $(\underline{y}^{opt}, \underline{\alpha}^{opt})$ using the algorithm described in [29, 6]. The problem on how to find the optimal number of pointwise sources m^{opt} will be discussed in Section 5.

4. The Method of Fundamental Solutions

The Method of Fundamental Solutions (MFS) is a meshless collocation method for the numerical solution of boundary value problems (BVP) with an available fundamental solution, see e.g., [7, 18, 22] and the references therein. In this case, the solution is sought as a linear combination of fundamental solutions with 'singularities' placed outside the domain. In this work, the

MFS is reformulated by taking singularities located outside and inside the domain. This approach allows an adequate representation of the pointwise sources, as well applies the MFS directly to the associated non-homogeneous BVP [1].

Definition 1. *Let $\Omega \subset \mathbb{R}^d$, with $d = 2, 3$, be a open and bounded domain. Consider the following problem*

$$\mathbb{L}[u(\underline{x})] = 0, \quad \underline{x} \in \mathbb{R}^d, \tag{30}$$

subject to a boundary condition given by

$$C[u(\underline{x})] = 0, \quad \underline{x} \in \partial\Omega, \tag{31}$$

where $\mathbb{L}$ is a linear differential operator and C denotes a Dirichlet, Neumann or Robin boundary condition [19]. The approximate solution $u_M(\underline{x})$ using the MFS for problem (30)-(31) is given by the following finite linear combination

$$u_M(\underline{x}) = \sum_{i=1}^{M} c_i \Phi(\underline{x}, \underline{P}_i), \quad \underline{x} \in \overline{\Omega}, \tag{32}$$

where $\underline{P}_i$ are the 'singularities' of the fundamental solution Φ of (30), which are located outside Ω. The coefficients c_i in Eq.(32), with $i = 1, \ldots, M$, can be determined by Eq.(31), that is, using collocation on $\partial\Omega$ and solving the associated linear system of equations.

The set of points $\underline{P}_i$, for $i = 1, \ldots, M$, belonging to the boundary $\widehat{\partial\Omega}$ of a set $\widehat{\Omega} \supset \Omega$, is also called *an external source points set*. The set of points $\underline{x}_k$, for $k = 1, \ldots, L$, on $\partial\Omega$ is called *a boundary collocation points set*. The boundary $\widehat{\partial\Omega}$ is called *the fictitious boundary* and the boundary $\partial\Omega$ from Ω is called *the physical boundary*. Figure 1 shows both physical and fictitious boundaries, with their respective external source points and boundary collocation points. The number and locations of collocation and source points are pre-assigned, adding some additional arbitrariness in the MFS.

The MFS can be used to properly represent a source b with m pointwise internal sources by inserting m source points inside the domain Ω. Consider the following Dirichlet direct problem for the modified Helmholtz equation:

$$\begin{cases} -\Delta u + \lambda u &= b \quad \text{in} \quad \Omega, \\ u &= u^* \quad \text{on} \quad \partial\Omega, \end{cases} \tag{33}$$

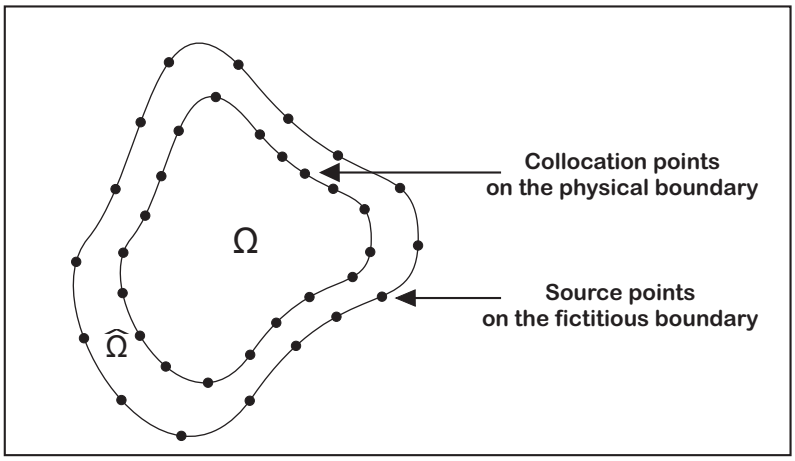

Figure 1: A MFS scheme applied to a boundary value problem.

where $\lambda > 0$ and the source b is given by

$$b(\underline{x}) = \sum_{j=1}^{m} \alpha_j \delta(\underline{x} - \underline{y}_j), \tag{34}$$

with m, α_j and $\underline{y}_j \in \Omega$ for $j = 1, \ldots, m$ being the number, intensities and locations of the pointwise sources that compound the source b. For the solution of (33) with b given by (34), using the MFS, we propose

$$u_{MFS}(\underline{x}) = \sum_{i=1}^{M} c_i \phi(||\underline{x} - \underline{P}_i||) + \sum_{j=1}^{m} \alpha_j \phi(||\underline{x} - \underline{y}_j||), \tag{35}$$

where $\phi(||\underline{x}||)$ is the fundamental solution of the modified Helmholtz equation given by

$$\phi(||\underline{x}||) = \frac{1}{2\pi} K_0(\sqrt{\lambda}||\underline{x}||), \tag{36}$$

in $\mathbb{R}^2$, and

$$\phi(||\underline{x}||) = \frac{e^{\sqrt{\lambda}||\underline{x}||}}{4\pi||\underline{x}||}, \tag{37}$$

in $\mathbb{R}^3$, with $K_0(||\underline{x}||)$ being the modified Bessel function of the second kind of zero order. For the Dirichlet boundary condition of the problem (33), we have

$$\sum_{i=1}^{M} c_i \phi(||\underline{x}_k - \underline{P}_i||) = u^*(\underline{x}_k) - \sum_{i=1}^{m} \alpha_i \phi(||\underline{x}_k - \underline{y}_i||), \tag{38}$$

where $\underline{x}_k$ are boundary collocation points on the physical boundary $\partial\Omega$ for $k = 1, ..., L$. Thus, we can find the approximate solution of (33) by solving the linear L algebraic equations (38), with M unknowns represented by the vector of coefficients $\underline{c} = (c_1, \ldots, c_M)$. The flux q^* can be easily obtained by calculating the normal derivative of equation (35) to give

$$\partial_n u_{MFS}(\underline{x}) = \sum_{i=1}^{M} c_i \partial_n \phi(||\underline{x} - \underline{P}_i||) + \sum_{j=1}^{m} \alpha_j \partial_n \phi(||\underline{x} - \underline{y}_j||). \tag{39}$$

This facility in calculating derivatives is, in fact, another advantage of the MFS. It is worth noting that the numerical solution of the direct problem associated with functions v_i, for $i = 1, \ldots, m$, presented in Subsection 3.1 is a particular case of the problem (33), where u^* is zero and b is a single point source of unit intensity.

Some works deal with the relationship between the MFS convergence and the fictitious values of the limit radius and the number of source points. In [3, 23, 24] it is possible to find error estimates for interior and exterior domain problems, which evidence the exponential convergence dependence with the number of source and collocation points. On the other hand, these parameters also make the condition number of the coefficient matrix resulting from the MFS grow exponentially. Besides the fictitious boundary radius value and number of source points, such estimates also depend on the domain dimension and its area or volume. For general considerations, the reader may also consult [11]. Finally, we stress that the combinatorial nature of the problem makes an exhaustive search quickly unfeasible when the number of point sources increases [28].

5. Numerical Results

5.1. 2D Case

In this subsection, we present four 2D examples. In all examples the set of admissible point source locations X is generated using a distribution of *sunflower seeds* [31]. The flux data q^* was generated numerically by solving

the direct problem using the MFS, as explained in Section 4, where $u|_{\partial\Omega}$ is given by

$$u|_{\partial\Omega} = u^*(x,y) = cos(x) \text{ for all } (x,y) = \underline{x} \in \partial\Omega. \tag{40}$$

The calculation of matrix H and vector $\underline{d}$, defined in (22) and (23), were performed using Simpson's 1/3 numerical integration technique with 25 points on the physical boundary $\partial\Omega$. Each pointwise source is represented by a circle, where its center corresponds to the location and its radius is proportional to its intensity.

The first example consists in performing the adjustment of the radius $R > 1$ of the fictitious boundary $\partial\widehat{\Omega}$ for two different values of λ. The second example illustrates the procedure for identifying the correct number of pointwise sources. The third example analyzes the influence of the size of the set X of admissible sources. For the sake of simplicity, in the first three examples, the domain Ω is the unit circle centered at the origin $\Omega = B_1(\underline{0})$. However, the fourth example reconstructs the pointwise sources considering noise in measured data q^* for a non-symmetric bean-shaped domain Ω.

Example 1

The objective of this example is to investigate the effect of the radius R of the MFS fictitious boundary $\partial\widehat{\Omega}$ for two different values of λ, namely $\lambda_1 = 9.5$ (large reaction) and $\lambda_2 = 1.0$ (moderate reaction). In both cases, we consider that the set of admissible point-source locations X has $m = 100$ points.

For $\lambda = \lambda_1 = 9.5$, the target to be reconstructed consists of a single pointwise source with intensity $\alpha^* = 10$ and located at $\underline{y}_1^* = (-0.11 + \Delta x, -0.22 - \Delta y)$, where $\Delta x = \Delta y = 0$ or $\Delta x = \Delta y = 0.05$. It is important to note that $\underline{y}_1^* \in X$ iff $\Delta x = \Delta y = 0$. We fix the numbers of boundary collocation and 'singularity' points as $L = L_1 = 15$ and $M = M_1 = 12$, respectively. In order to evaluate the accuracy of reconstruction, the relative error E between target intensity α^* and optimal intensity α^{opt} is calculated, namely,

$$E = \frac{|\alpha^{opt} - \alpha^*|}{|\alpha^*|} \times 100. \tag{41}$$

Figure 2(a) shows the variation of such relative error E as radius R of the fictitious boundary is increased and corresponds to the case where $\Delta x = \Delta y = 0$, i.e. $\underline{y}_1^* \in X$. Observing the relative error, it is possible to conclude that a reconstruction of the intensity is almost exact. In addition, obtained

optimal location $\underline{y}^{opt}$ matches the exact location $\underline{y}_1^*$, i.e., $\|\underline{y}^{opt} - \underline{y}_1^*\| = 0$. For the case where $\underline{y}_1^* \notin X$, we can observe in Figure 2(b) that the relative error is stable for $R \geq 1.2$, attaining values close to 5%. Moreover, by calculating the Euclidean norm of the localization error, we have obtained $\|\underline{y}^{opt} - \underline{y}_1^*\| < 0.07$ for $R \geq 1.2$.

For $\lambda = \lambda_2 = 1.0$, the target considered also contains only one pointwise source located at $\underline{y}_1^* = (-0.39 + \Delta x, 0.43 - \Delta y)$ with intensity $\alpha^* = 20$. In this case, we take $L = L_2 = 15$ boundary collocation points and $M = M_2 = 16$ 'singularity' points. The analysis of quality of reconstruction is analogous to what was previously obtained in Figures 2(a) and 2(b) for $\lambda = \lambda_1 = 9.5$. As we can see in Figures 2(c) and 2(d), the same behaviors can be observed with respect to the reconstruction of the intensity, except for the region where some oscillations occur in the case where $\underline{y}_1^* \in X$. Regarding the locations, the results obtained are similar.

In the subsequent examples 2-4, we consider $\lambda = 9.5$, $L = L_1 = 15$ and $M = M_1 = 16$. In order to avoid committing an inverse crime, we consider $R = 2$ to obtain the flux from the direct problem and $R = 3$ in the inverse reconstruction algorithm.

Example 2

In this example, the objective is to reconstruct a target source with three pointwise sources ($m^* = 3$), whose locations are given by $\underline{y}_1^* = (-0.39, 0.43)$, $\underline{y}_2^* = (-0.45, -0.34)$ and $\underline{y}_3^* = (0.57, 0.40)$, with same intensities: $\alpha_1^* = \alpha_2^* = \alpha_3^* = 6$. Figure 3 shows the target to be reconstructed. The optimization problem has a different solution for each value of m. In this example, we propose a method to determine the correct number of pointwise sources m^{opt}. Initially, the reconstruction method looks for a solution with one point source ($m = 1$) and proceeds to increase value of m until the vector of optimal intensities $\underline{\alpha}^{opt}$ contains one entry with negligible value. Figure 4 illustrates the results obtained for each value of m. As expected, the reconstruction is exact when $m = m^* = 3$, i.e., $\underline{y}_i^{opt} = \underline{y}_i^*$ and $\alpha_i^{opt} = \alpha_i^*$ for all $i \in \{1, 2, 3\}$. In addition, for $m = 4$, the vector of optimal intensities has four entries, where three of them coincide with the entries obtained when $m = 3$ and the fourth entry has negligible value in relation to the others. This situation can also be seen in Figure 5 which illustrates the value of the functional $\mathcal{J}$, given by Eq.(6), for each value of m. Note that for $m = 3$ the functional vanishes, as expected by Proposition 1. Therefore, we can conclude that the correct number of pointwise sources is $m^{opt} = 3$. Table 1 shows the entries of the

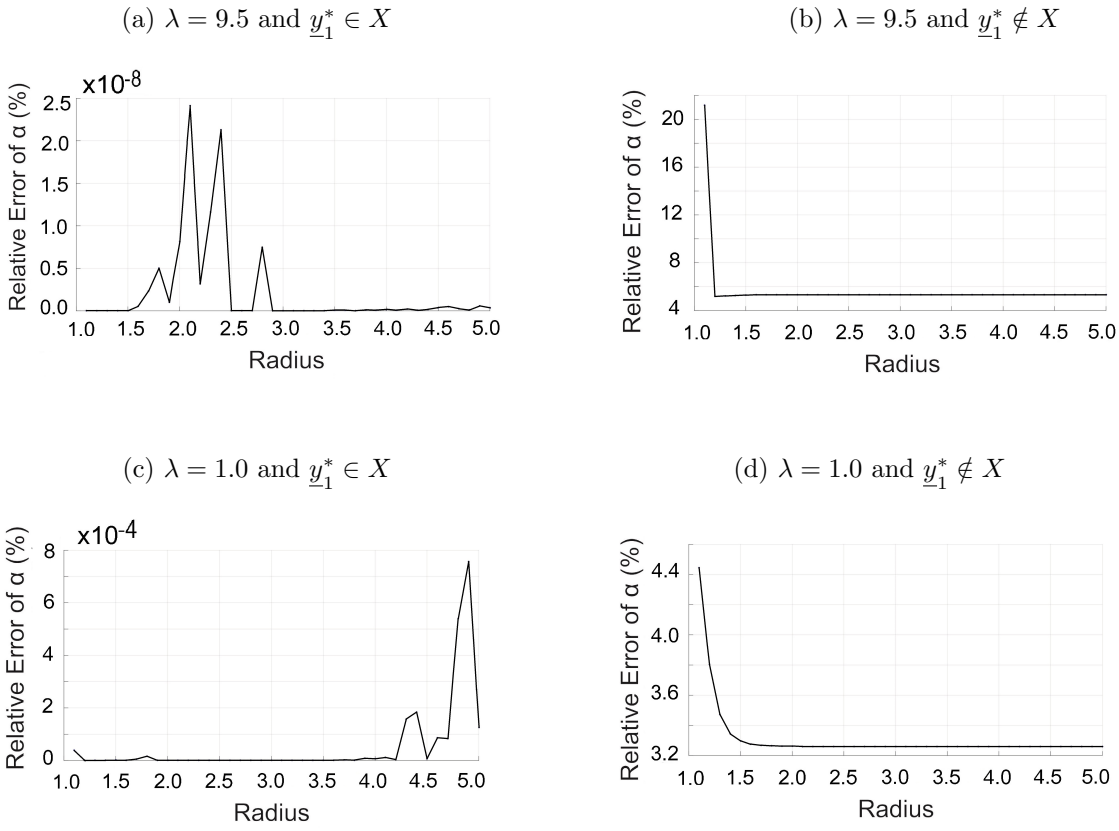

Figure 2: Example 1: Radius R of the fictitious boundary versus the relative error E.

vector of optimal intensities for different values of m.

Table 1: Example 2: The vector $\underline{\alpha}_m^{opt}$ of optimal intensities for different values of m.

m	$\underline{\alpha}_m^{opt}$
1	38.618
2	(5.2421, 20.736)
3	(6.0000, 6.0000, 6.0000)
4	(6.0000, 6.0004, 5.9989, 0.0002)

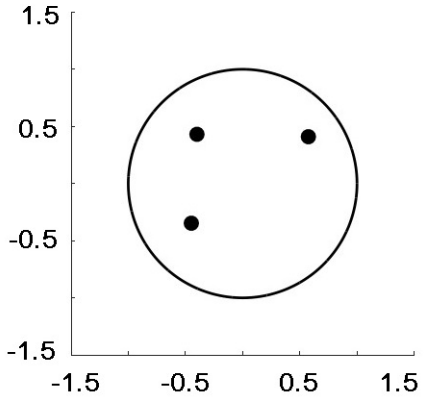

Figure 3: Example 2: Target.

Example 3

This example aims to analyze the sensitivity of the reconstruction method concerning the size of the set of admissible locations X. Let us consider the reconstruction of a source with a single pointwise source located at $\underline{y}_1^* = (0.25, -0.32)$ with intensity $\alpha^* = 10$. Four different sizes are considered for the set X, namely $\#X \in \{20, 100, 200, 500\}$. In addition to the optimal intensities and locations, Table 2 also shows the distance between the optimal and target locations, as well as the relative error (41). Note that results get more accurate as of the size of X increases.

Table 2: Example 3: Results obtained for different sizes of the set of admissible locations.

$\#X$	$\underline{y}^{opt}$	$\left\|\underline{y}^{opt} - \underline{x}^*\right\|$	α^{opt}	E
20	$(0.40, -0.25)$	0.1673	7.8314	21.6%
100	$(0.29, -0.29)$	0.0530	9.6264	3.7%
200	$(0.21, -0.32)$	0.0390	10.354	3.5%
500	$(0.24, -0.33)$	0.0180	9.7806	2.1%

Example 4

In this example, the reconstruction behavior for noisy data is analyzed. Instead of using the pair (u^*, q^*) to perform the reconstruction, we corrupt the Neumann data by noise and invert the pair (u^*, q_μ^*). The noisy measured

data is $q^*_\mu = q^*(1 + \mu\eta)$, where η is a function that generates random values in the interval $[-1, 1]$ and μ corresponds to the noise level. Dirichlet data u^* can also be corrupted by noise. The considered noise is multiplicative but additive noise can also be simulated. In fact, one advantage of the gradient-based method of Section 2.2 has over statistical methods of optimization is that it does not require any assumption on the type of noise the data is contaminated with. The solution domain Ω, illustrated by Figure 6, is the bean-shaped domain, given by the radial parameterization

$$r(\theta) = \frac{0.55 + 0.30\,cos(\theta) + 0.1\,sin(2\theta)}{0.6 + 0.3\,cos(\theta)}, \quad \theta \in (0, 2\pi]. \tag{42}$$

The target contains three pointwise sources located at $\underline{y}^*_1 = (0.72, 0.30)$, $\underline{y}^*_2 = (-0.38, 0.26)$ and $\underline{y}^*_3 = (0.46, -0.54)$, with intensities $\alpha^*_1 = 5$, $\alpha^*_2 = 10$ and $\alpha^*_3 = 15$. Table 3 shows the results obtained for the following noise levels: $\mu = 5\%$, $\mu = 10\%$ and $\mu = 20\%$, where E_i represents the error, given by Eq. (41), of component i. From this table it can be seen that the reconstruction of $\underline{\alpha}^{opt}$ is close to the exact value $(5, 10, 15)$ when up to 10% noisy data are inverted. For higher level of noise such as 20% the reconstruction starts to significantly deteriorate.

Table 3: Example 4: Results obtained for different levels of noise.

μ	$\underline{\alpha}^{opt}$	$\sum_{i=1}^{3} E_i$
0%	(5.0003,10.0014,14.9993)	0.02%
5%	(4.9514,10.2605,15.1807)	4.78%
10%	(5.1044,11.0354,14.0925)	18.49%
20%	(5.6081,16.9403,3.8614)	155.82%

5.2. 3D Case

We also show four examples for the three-dimensional case with the same purposes as the previous 2D case. The domain Ω is given by the unit sphere centered at the origin. On the boundary, we prescribe homogeneous Dirichlet data and the corresponding Neumann data q^* is generated as explained in Section 4. For the numerical solution of auxiliary problems, the pointwise sources are distributed over the boundary of a sphere centered at the origin whose radius and the number of 'singularity' points are adjusted for different values of λ. In addition, an adjustment is also made for the

number of collocation points on the boundary, where the implementations `sphere_cubed_point_num`, `sphere_cubed_points` and `sphere_cubed_points_face` [5] are used to generate points on the physical and fictional boundaries of the direct problems. Figure 7 illustrates a simulation of the distribution of source and collocation points using a radius $R = 2$ for the fictitious boundary, with 53 points on both boundaries. The set of admissible source locations is computed by the implementations `grid_ball` and `grid_ball_count` [4]. The Hessian matrix H and the vector $\underline{d}$ are calculated by evaluating the surface integrals using the implementation `getLebedevSphere` [30] based on the Lebedev quadrature [27].

Example 5

As in Example 1, in this example the radius R of the fictitious boundary is adjusted for a given λ in a three-dimensional domain. Thus, taking initially $\lambda_1 = 9.5$, we perform the reconstruction of a single pointwise source at location $\underline{y}_1^* = (-0.66 + \Delta x, -0.33 - \Delta y, -0.33 + \Delta z)$, with $\Delta x, \Delta y, \Delta z \in \{0.00, 0.05\}$ and intensity $\alpha^* = 2$, in order to analyze the behavior of the method according to the changes in the radius R, in cases where $\underline{y}_1^* \in X$, when $\Delta x = \Delta y = \Delta z = 0$, and $\underline{y}_1^* \notin X$ when $\Delta x = \Delta y = \Delta z = 0.05$. The number of points in the set of admissible source locations is fixed at 117. Setting $L = L_1 = 26$ collocation points and $M = N_1 = 56$ source points, the reconstruction method provides very satisfactory results. Figures 8(a) and 8(b) show relative error of intensity reconstruction considering $\underline{y}_1^* \in X$ and $\underline{y}_1^* \notin X$, respectively. Note that for $R = 1.5$ in Figure 8(b), the error stabilizes around 8%. However, the error in Figure 8(a) is around 10^{-7}% for $R \in [2.6, 4.3]$. The location is reconstructed exactly when $\underline{y}_1^* \in X$ and with error $\|\underline{y}^{opt} - \underline{y}_1^*\| = 0.0866$ when $\underline{y}_1^* \notin X$ for all $R \in [1.1, 5]$.

For $\lambda_2 = 1.0$, taking $L = L_2 = 26$ and $N = N_2 = 56$, we also reconstruct a single pointwise source, located at $\underline{y}_1^* = (0.33 + \Delta x, -0.33 - \Delta y, 0.66 + \Delta z)$, with intensity of $\alpha^* = 4$. Figures 8(c) and 8(d), respectively, show the relative error of α in cases where $\underline{y}_1^* \in X$ and $\underline{y}_1^* \notin X$. Note that the curve in Figure 8(d) begins to stabilize from $R = 2$, with error close to 12%. In Figure 8(c), the error was obtained around 10^{-16}% for $R \in [1.1, 3.4] \cup [4, 5]$. With respect to the pointwise source location, the results are analogous to the case when $\lambda = \lambda_1 = 9.5$.

Example 6

In this example, considering $\lambda = \lambda_1 = 9.5$, the source to be reconstructed contains three pointwise sources located at $\underline{y}_1^* = (0.00, 0.34, 0.34)$, $\underline{y}_2^* = (-0.34, 0.00, -0.34)$ and $\underline{y}_3^* = (0.68, 0.34, -0.34)$, with intensities $\alpha_1^* = \alpha_2^* = \alpha_3^* = 8$. The procedure used to obtain the correct number of sources is analogous to that performed in Example 2. Figure 9 shows the results obtained for $m \in \{1, 2, 3, 4\}$. For $m = 4$, the method reconstructs a fourth source with negligible intensity (see Table 4). Thus, one can conclude that the correct number of pointwise sources is $m^{opt} = 3$.

Table 4: Example 6: Results obtained for different values of m, for $\lambda = \lambda_1 = 9.5$.

m	$\underline{\alpha}_m^{opt}$
1	36.630
2	(7.3595,23.767)
3	(8.0000,8.0000,7.9999)
4	(8.0000,7.9999,8.0000,0.0000)

Taking $\lambda = \lambda_2 = 1.0$, we consider the same locations of the sources previously studied, with intensities $\alpha_1^* = 3$, $\alpha_2^* = 8$ and $\alpha_2^* = 13$. Table 5 shows numerical results and Figure 10 illustrates geometrical results obtained for each value of m. Note that the method reconstructs three pointwise sources of close intensities for $m = 3$ and $m = 4$. In addition, a fourth source with negligible intensity is obtained for $m = 4$, setting the method's stopping criterion. The locations of the sources for $m = 3$ are reconstructed exactly.

Table 5: Example 6: Results obtained for different values of m, for $\lambda = \lambda_2 = 1.0$.

m	$\underline{\alpha}^{opt}$
1	20.096
2	(14.314,9.7602)
3	(12.9999,8.0000,3.0000)
4	(12.8650,7.8493,2.6605,0.6130)

Example 7

In order to analyze the reconstruction of source in the presence of noise, we consider three pointwise sources located at $\underline{y}_1^* = (0.00, 0.27, 0.27)$, $\underline{y}_2^* = -(0.00, 0.81, 0.27)$ and $\underline{y}_3^* = -(0.54, 0.54, 0.27)$, with intensities $\alpha_1^* = 5$, $\alpha_2^* =$

10 and $\alpha_3^* = 15$. Let us take first $\lambda = \lambda_1 = 9.5$. The Neumann data q^* is corrupted with noise in the same manner as Example 4, with noise levels $\mu = 0\%, 5\%, 10\%$ and 20%. Table 6 contains the results for intensities on each noise level. It is observed that the reconstructed intensities do not present great differences in relation to their exact values considering up to 10% noise.

Table 6: Example 7: Results obtained for different levels of noise, for $\lambda = \lambda_1 = 9.5$.

μ	$\underline{\alpha}^{opt}$	$\sum_{i=1}^{3} E_i$
0%	(4.9999,10.0001,15.0021)	0.02%
5%	(5.0543,9.8340,15.4140)	5.51%
10%	(5.1831,9.4872,16.1300)	16.32%
20%	(5.2454,14.1235,5.9912)	106.20%

Performing the same procedure for $\lambda = \lambda_2 = 1.0$, we consider the same locations of the sources previously used, taking now an intensity of $\alpha^* = 5$ for all of them. Table 7 shows the results obtained. Note that, again, the reconstructed intensities do not present discrepancies in relation to their exact values. Locations are reconstructed exactly for both $\lambda = \lambda_1 = 9.5$ and $\lambda = \lambda_2 = 1.0$.

Table 7: Example 7: Results obtained for different levels of noise, for $\lambda = \lambda_2 = 1.0$.

μ	$\underline{\alpha}^{opt}$	$\sum_{i=1}^{3} E_i$
0%	(5.0000,4.9999,4.9999)	$0,004\%$
5%	(5.0396,5.0365,4.9747)	$2,03\%$
10%	(5.1433,5.0874,4.9617)	$5,38\%$
20%	(4.5836,5.6699,4.5572)	$30,58\%$

6. Conclusions

The main purpose of this paper was to reconstruct the location and the intensity of a set of pointwise sources, given by a linear combination of Dirac-delta functions, from Cauchy data on the boundary of the solution domain for a model given by the modified Helmholtz equation. The strategy used to solve the inverse source problem consisted in defining an equivalent optimization problem and performing a sensitivity analysis of the associated least-squares

functional, which led us to a strictly convex problem with respect to the intensity vector.

Next, we have proposed a reconstruction algorithm based on the MFS. Furthermore, by considering source points inside the domain, we have applied the MFS directly to the homogeneous and non-homogeneous associated direct problems.

We have performed several numerical tests to evaluate the algorithm in relation to grid size, the number of 'singularities' and placement points, and the distance between the fictitious and physical boundaries. Several examples have been investigated for two and three-dimensional problems showing that the proposed algorithm is accurate (for exact data) and stable (for noisy data). Future work will concern extending the results obtained for models given by other linear PDEs.

Acknowledgements

This research was supported by CAPES (Brazilian Higher Education Staff Training Agency) through the project with grant number 88882.317919/2013-01. This support is gratefully acknowledged.

Conflict of interest

The authors certify that they have NO affiliations with or involvement in any organization or entity with any financial interest or non-financial interest in the subject matter or materials discussed in this manuscript.

References

[1] C. Alves and C. Chen. A new method of fundamental solutions applied to nonhomogeneous elliptic problems. *Advances in Computational Mathematics*, 23(1-2):125–142, 2005.

[2] C. J. Alves and A. L. Silvestre. On the determination of point-forces on a Stokes system. *Mathematics and computers in Simulation*, 66(4-5):385–397, 2004.

[3] A. H. Barnett and T. Betcke. Stability and convergence of the method of fundamental solutions for Helmholtz problems on analytic domains. *Journal of Computational Physics*, 227(14):7003–7026, 2008.

[4] J. Burkardt. Grid points within a 3d ball. https://people.sc.fsu.edu/~jburkardt/m_src/ball_grid/ball_grid.html, 2010. (Accessed on 03/09/2018).

[5] J. Burkardt. Grids on a sphere. https://people.sc.fsu.edu/~burkardt/m_src/sphere_grid/sphere_grid.html, 2012. (Accessed on 18/09/2018).

[6] A. Canelas, A. Laurain, and A. A. Novotny. A new reconstruction method for the inverse source problem from partial boundary measurements. *Inverse Problems*, 31(7):075009, 2015.

[7] P. Carvalho, A. Doubova, E. Fernández-Cara, and J. Rocha de Faria. Some new results for geometric inverse problems with the method of fundamental solutions. *Inverse Problems in Science and Engineering*, 29(1):131–152, 2021.

[8] E. Casas. Control of an elliptic problem with pointwise state constraints. *SIAM Journal on Control and Optimization*, 24(6):1309–1318, 1986.

[9] E. Casas, C. Clason, and K. Kunisch. Parabolic control problems in measure spaces with sparse solutions. *SIAM Journal on Control and Optimization*, 51(1):28–63, 2013.

[10] C. Chen, X. Jiang, W. Chen, and G. Yao. Fast solution for solving the modified Helmholtz equation with the method of fundamental solutions. *Communications in Computational Physics*, 17(3):867–886, 2015.

[11] A. H. Cheng and Y. Hong. An overview of the method of fundamental solutions—solvability, uniqueness, convergence, and stability. *Engineering Analysis with Boundary Elements*, 120:118–152, 2020.

[12] L. de Rochefort, T. Liu, B. Kressler, J. Liu, P. Spincemaille, V. Lebon, J. Wu, and Y. Wang. Quantitative susceptibility map reconstruction from mr phase data using Bayesian regularization: validation and application to brain imaging. *Magnetic Resonance in Medicine*, 63(1):194–206, 2010.

[13] A. El Badia and T. Ha-Duong. Determination of point wave sources by boundary measurements. *Inverse Problems*, 17(4):1127–1139, 2001.

[14] A. El Badia and T. Ha-Duong. On an inverse source problem for the heat equation. application to a pollution detection problem. *Journal of Inverse and Ill-posed Problems*, 10(6):585–599, 2002.

[15] A. El Badia, T. Ha-Duong, and A. Hamdi. Identification of a point source in a linear advection–dispersion–reaction equation: application to a pollution source problem. *Inverse Problems*, 21(3):1121–1136, 2005.

[16] A. El Badia and T. Nara. An inverse source problem for Helmholtz's equation from the Cauchy data with a single wave number. *Inverse Problems*, 27(10):105001 (15pp), 2011.

[17] A. Hamdi. Identification of point sources in two-dimensional advection-diffusion-reaction equation: application to pollution sources in a river. Stationary case. *Inverse Problems in Science and Engineering*, 15(8):855–870, 2007.

[18] Y. Hon and T. Wei. A fundamental solution method for inverse heat conduction problem. *Engineering Analysis with Boundary Elements*, 28(5):489–495, 2004.

[19] G. Houzeaux and R. Codina. A chimera method based on a Dirichlet/Neumann (Robin) coupling for the Navier–Stokes equations. *Computer Methods in Applied Mechanics and Engineering*, 192(31-32):3343–3377, 2003.

[20] W. Hui and Q. Qinghua. Some problems with the method of fundamental solution using radial basis functions. *Acta Mechanica Solida Sinica*, 20(1):21–29, 2007.

[21] B. Jin and Y. Zheng. A meshless method for some inverse problems associated with the Helmholtz equation. *Computer Methods in Applied Mechanics and Engineering*, 195(19-22):2270–2288, 2006.

[22] A. Karageorghis, D. Lesnic, and L. Marin. A survey of applications of the MFS to inverse problems. *Inverse Problems in Science and Engineering*, 19(3):309–336, 2011.

[23] M. Katsurada. Asymptotic error analysis of the charge simulation method. *Journal of the Faculty of Science, University of Tokyo, Section 1A*, 37:635–657, 1990.

[24] M. Katsurada. Charge simulation method using exterior mapping functions. *Japan Journal of Industrial and Applied Mathematics*, 11(1):47–61, 1994.

[25] A. D. Klose, V. Ntziachristos, and A. H. Hielscher. The inverse source problem based on the radiative transfer equation in optical molecular imaging. *Journal of Computational Physics*, 202(1):323–345, 2005.

[26] C. Le Niliot and F. Lefevre. Multiple transient point heat sources identification in heat diffusion: application to numerical two-and three-dimensional problems. *Numerical Heat Transfer: Part B: Fundamentals*, 39(3):277–301, 2001.

[27] V. I. Lebedev and D. Laikov. A quadrature formula for the sphere of the 131st algebraic order of accuracy. In *Doklady Mathematics*, volume 59, pages 477–481. Pleiades Publishing, Ltd., 1999.

[28] T. J. Machado, J. S. Angelo, and A. A. Novotny. A new one-shot pointwise source reconstruction method. *Mathematical Methods in the Applied Sciences*, 40(5):1367–1381, 2017.

[29] P. Menoret, M. Hrizi, and A. Novotny. On the Kohn–Vogelius formulation for solving an inverse source problem. *Inverse Problems in Science and Engineering*, 29(1):56–72, 2021.

[30] R. Parrish. getlebedevsphere. `https://www.mathworks.com/matlabcentral/fileexchange/27097-getlebedevsphere`, 2010. (Accessed on 03/09/2018).

[31] H. Vogel. A better way to construct the sunflower head. *Mathematical Biosciences*, 44(3-4):179–189, 1979.

[32] V. Winiarek, M. Bocquet, O. Saunier, and A. Mathieu. Estimation of errors in the inverse modeling of accidental release of atmospheric pollutant: Application to the reconstruction of the cesium-137 and iodine-131 source terms from the Fukushima Daiichi power plant. *Journal of Geophysical Research: Atmospheres*, 117(D5):1–16, 2012.

[33] O. Zienkiewicz and R. Taylor. *The Finite Element Method: The Basis*, volume 1. Butterworth-Heinemann, Oxford, V edition, 2000.

(a) $m = 1$.

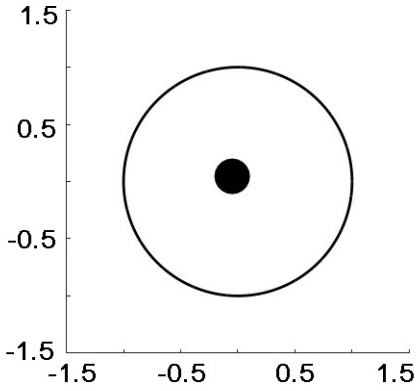

(b) $m = 2$.

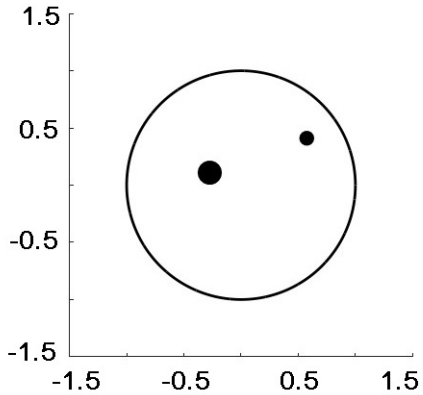

(c) $m = 3$.

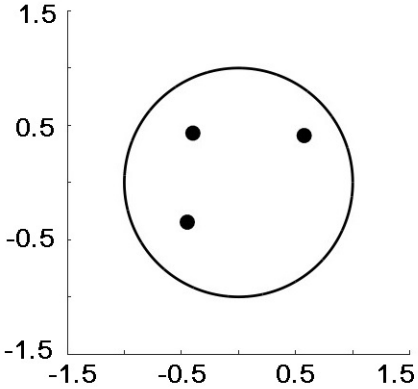

(d) $m = 4$.

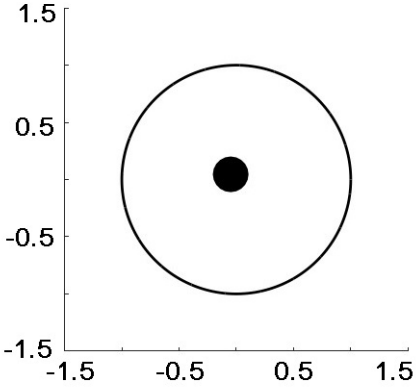

Figure 4: Example 2: Reconstructed sources for different values of m.

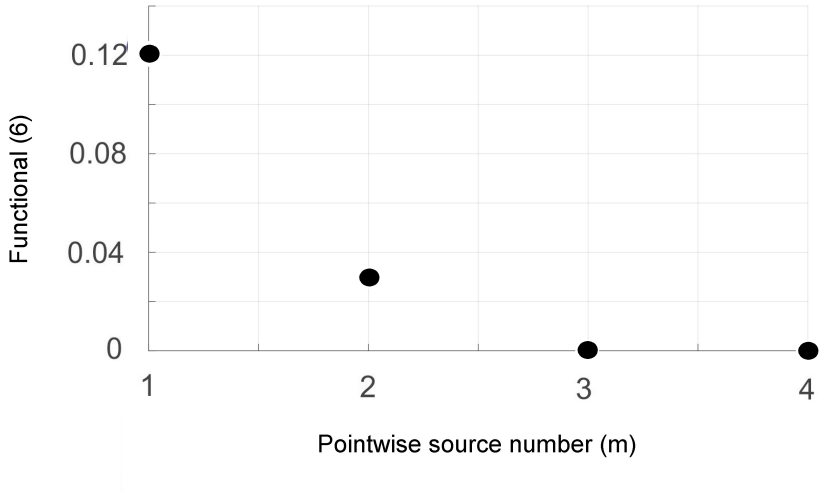

Figure 5: Example 2: Number of pointwise sources (m) versus the values of least-squares functional (6).

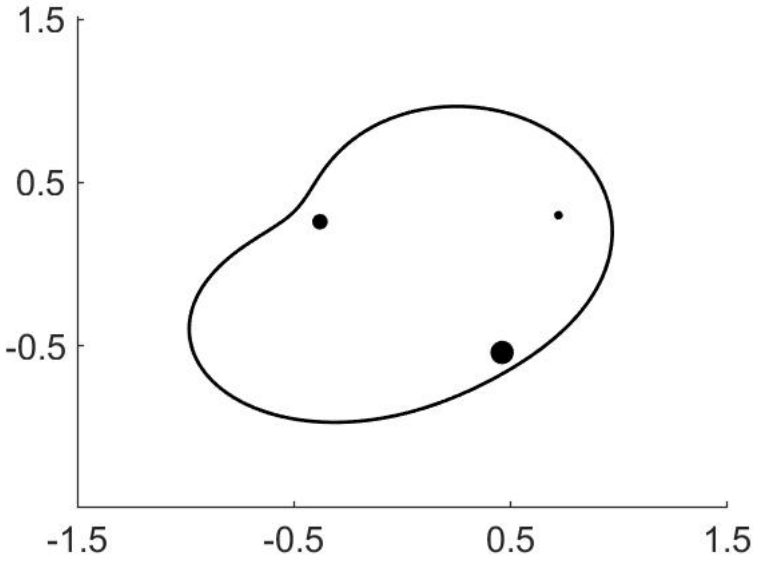

Figure 6: Example 4: Target.

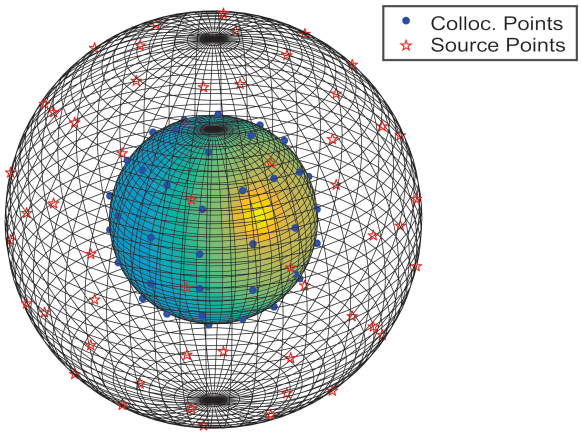

Figure 7: Distribution of source and collocation points on the physical and fictitious boundaries.

(a) $\lambda = 9.5$ and $\underline{y}_1^* \in X$

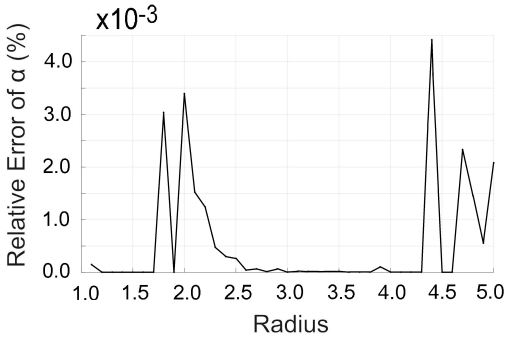

(b) $\lambda = 9.5$ and $\underline{y}_1^* \notin X$

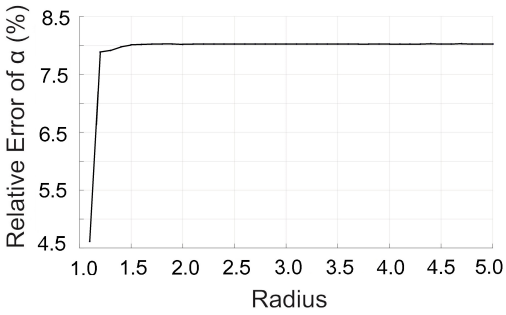

(c) $\lambda = 1.0$ and $\underline{y}_1^* \in X$

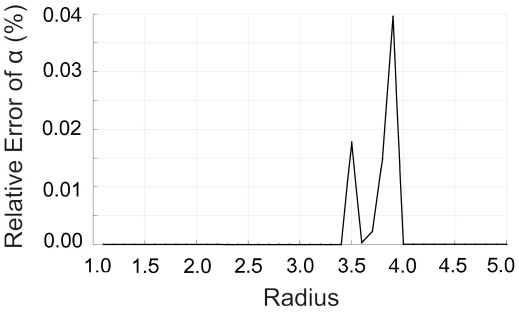

(d) $\lambda = 1.0$ and $\underline{y}_1^* \notin X$

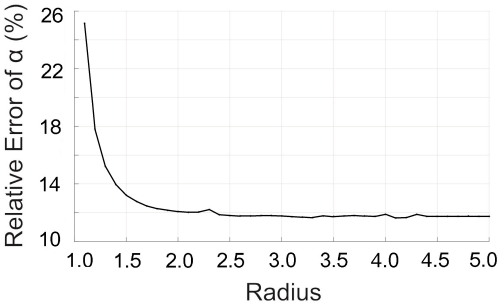

Figure 8: Example 5: Radius R of the fictitious boundary versus the relative error (41).

(a) $m = 1$; $\lambda = 9.5$.

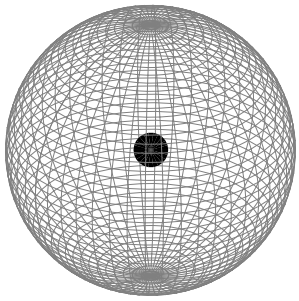

(b) $m = 2$; $\lambda = 9.5$.

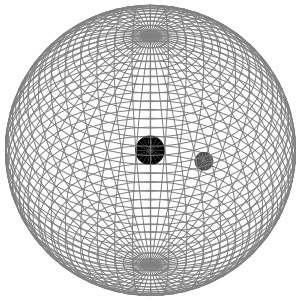

(c) $m = 3$; $\lambda = 9.5$.

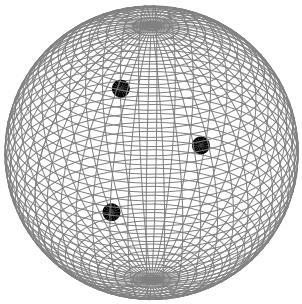

(d) $m = 4$; $\lambda = 9.5$.

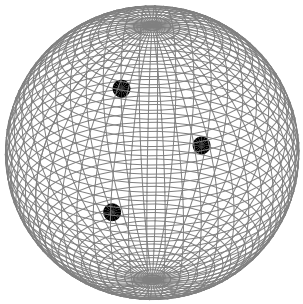

Figure 9: Example 6: Reconstructed sources for different values of m and large reaction $\lambda = 9.5$.

(a) $m = 1$; $\lambda = 1.0$.

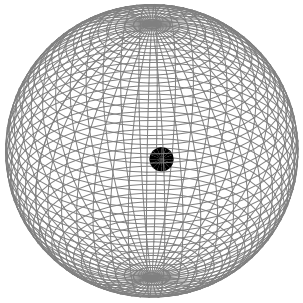

(b) $m = 2$; $\lambda = 1.0$.

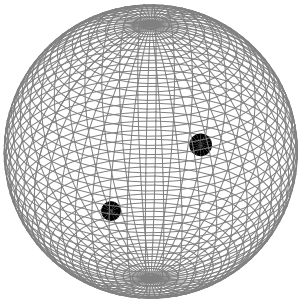

(c) $m = 3$; $\lambda = 1.0$.

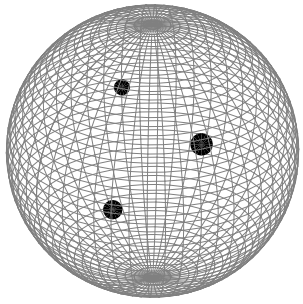

(d) $m = 4$; $\lambda = 1.0$.

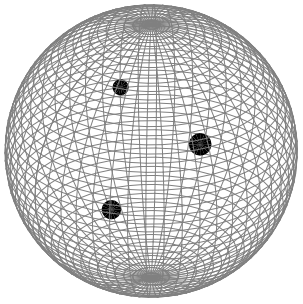

Figure 10: Example 6: Reconstructed sources for different values of m and moderate reaction $\lambda = 1.0$.